Observer-based Angle of Attack Estimation for Tilt-Wing eVTOL Aircraft

Kentaro YOKOTA, Hiroshi FUJIMOTO
The University of Tokyo
5-1-5, Kashiwanoha, Kashiwa, Chiba, 277-8561, Japan
+81-4-7136-3881
yokota.kentaro19@ae.k.u-tokyo.ac.jp, fujimoto@k.u-tokyo.ac.jp

Hiroshi KOBAYASHI
Japan Aerospace Exploration Agency
6-13-1, Osawa, Chofu, Tokyo, 181-0015, Japan
+81-50-3362-2722
kobayashi.hiroshi2@jaxa.jp

***Abstract*—Research and development have been very active in electric vertical takeoff and landing (eVTOL) aircraft. Tilt-Wing aircraft especially receive significant attention as one of the most efficient configurations; however, they are apt to be unstable during the transition from hover to cruise. The angle of attack (AoA) is a critical parameter for aircraft motion, and with its real-time data, Tilt-Wing aircraft would achieve a more robust transition. Conventional methods of obtaining AoA require either additional sensors or an aircraft model, which is not robust to propeller slipstreams and unsuitable for Tilt-Wing aircraft. In this paper, a new AoA estimation method for Tilt-Wing aircraft is proposed. The proposed method is based on the propeller dynamics model and requires only an existing pitot tube. Wind tunnel tests verify its effectiveness.**

***Index Terms*—eVTOL, Tilt-Wing, angle of attack, estimation, observer**

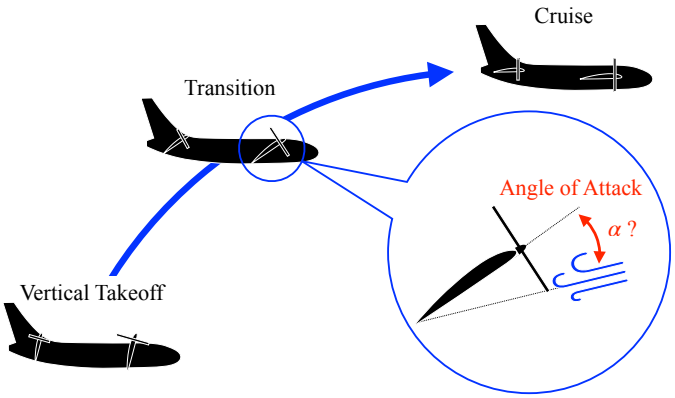

Fig. 1. Angle of attack of Tilt-Wing aircraft.

I. Introduction

A. Electric Flying Mobility

Research and development have been very active in electric flying mobility (EFM), such as electric vertical takeoff and landing (eVTOL) aircraft, because of the increasing demand for personal and eco-friendly aviation. Since EFM is powered by electric motors, it has the following advantages from the control engineering viewpoint:

1) Motor torque generation is 100 times faster than that of internal combustion engines [1].
2) Motor torque measurement is accurate [1].
3) Distributed installation (DEP: distributed electric propulsion) and independent control of motors are easy [2].
4) Power regeneration is possible [3].

These advantages enable EFM to achieve more secure, more efficient, and more eco-friendly aviation.

The authors' research group has been studying new control methods of propeller-driven electric aircraft, and proposed quick thrust and lift control methods [4], [5] and range extension systems [6] by adopting the motion control theories developed in the automotive industry [7].

B. eVTOL

eVTOL aircraft are currently receiving serious interest as one of the major EFM and are expected to play a significant role in future urban air transportation. A few examples of passenger eVTOL aircraft under development are CityAirbus (Airbus), Vahana (Airbus), Ehang 216 (Ehang), Lilium Jet (Lilium), S-A1 (Uber Elevate), Bell Nexus 4EX (Bell), and SD-XX (SkyDrive). Most of them can be categorized into four types: Multicopter, Lift + Cruise, Tilt-Rotor, and Tilt-Wing [8]. The differences in the configurations between these four are as follows: Multicopter has only upward thrusters, but Lift + Cruise has both upward and forward thrusters for hover and cruise, respectively. Tilt-Rotor and Tilt-Wing use the same thrusters for hover and cruise by tilting actuators, allowing them to vertically take off and land like helicopters and cruise like airplanes. Tilt-Wing has tilting wings with thrusters, but Tilt-Rotor has only tilting thrusters.

Compared to Multicopter, eVTOL aircraft with fixed-wing (e.g., Tilt-Rotor and Tilt-Wing) enable high-speed and efficient cruise. Also, Tilt-Rotor and Tilt-Wing need fewer actuators than Lift + Cruise. In particular, Tilt-Wing has aerodynamic advantages over Tilt-Rotor because the propeller slipstreams are not disturbed by the tilting wings [9].

C. Transition of Tilt-Wing eVTOL

One of the most significant difficulties in the flight of Tilt-Wing aircraft is the transition from hover to cruise. Since the aerodynamic characteristics of the tilting wings and tilting thrusters are complex and Tilt-Wing aircraft in the transition state are not similar to either helicopters or airplanes, they are apt to be unstable. Many studies have been conducted on

TABLE I
NOMENCLATURE

Symbol	Definition	Unit
α	Angle of attack (AoA)	rad, deg
ρ	Air density	$\mathrm{kg\,m^{-3}}$
σ	Tilt angle	rad, deg
n	Rotational speed of propeller	rps
B_ω	Viscosity coefficient of motor	$\mathrm{N\,m\,s\,rad^{-1}}$
C_F	Thrust coefficient of propeller	–
C_Q	Torque coefficient of propeller	–
D_p	Propeller diameter	m
F	Propeller thrust	N
J	Advance ratio	–
J_ω	Inertia moment of propeller	$\mathrm{kg\,m^2}$
J_n	Normal advance ratio	–
Q	Counter torque of propeller	N m
T	Input toque of motor	N m
T_C	Coulomb friction of motor	N m
V	Airspeed	$\mathrm{m\,s^{-1}}$
V_n	Normal airspeed	$\mathrm{m\,s^{-1}}$
V_{pitot}	Measured value by pitot tube	$\mathrm{m\,s^{-1}}$
V_x	x-axis airspeed	$\mathrm{m\,s^{-1}}$

this problem [10]–[13]. NASA has investigated the limitations of tilt angle and airspeed using experimental UAV GL-10 [10], [11]. Also, JAXA has proposed a gain-scheduled control method for quad Tilt-Wing UAV AKITSU [12].

D. Angle of Attack Estimation

The angle of attack (AoA), shown in Fig. 1, is a critical parameter in aircraft motion. The lift, for instance, changes by AoA. Therefore, with the real-time data of AoA, Tilt-Wing aircraft would achieve a more robust transition.

There are a few ways to obtain AoA. One way is airflow measurement [14]. However, it requires additional sensors, and such kinds of sensors are usually non-standard equipment for personal aircraft. Another way is a model-based estimation. Many estimation methods have proposed [15]–[19]; however, most of them are based on attitude and velocity measurement and aircraft model and are not robust to propeller slipstreams, which are difficult to be modeled. This problem becomes non-negligible with DEP, which takes advantage of slipstreams for motion control. Therefore, they cannot be applied to Tilt-Wing aircraft, and a new AoA estimation method is necessary for the stable transition.

E. About This Paper

The purpose of this paper is to propose a new AoA estimation method for Tilt-Wing aircraft without using additional sensors. This paper is organized as follows: Section II describes the modeling of Tilt-Wing aircraft. The new AoA estimation method is proposed in Section III. Finally, the experiment is discussed in Section IV.

The nomenclature used in this paper is shown in Table I.

II. Modeling

In this section, Tilt-Wing aircraft is modeled with a particular focus on the propeller and wing dynamics.

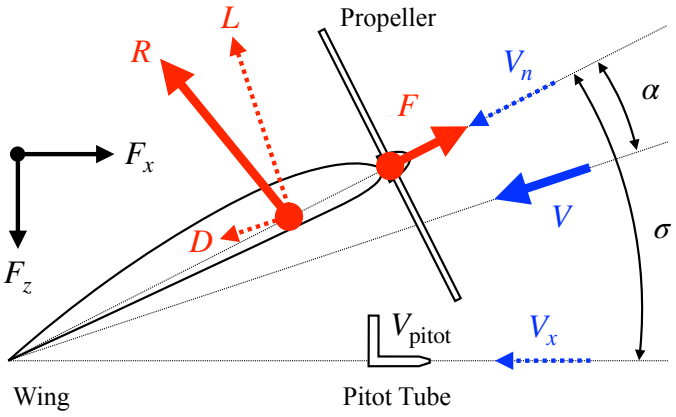

Fig. 2. Velocities and forces acting on wing and propeller.

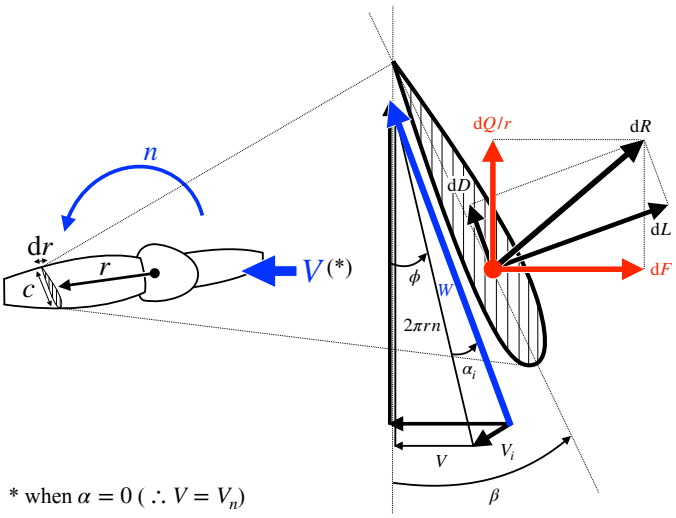

Fig. 3. Velocities and forces acting on propeller blade element.

A. Airspeed

Fig. 2 shows velocities and forces acting on the wing and propeller. V_n is normal to the propeller, and V_x is parallel to the pitot tube. Thus,

$$V_n = V\cos\alpha, \tag{1}$$
$$V_x = V\cos(\sigma - \alpha). \tag{2}$$

B. Propeller

Fig. 3 shows velocities and forces acting on the propeller blade element when $\alpha = 0$. The blade element is r away from the center and has a thickness of $\mathrm{d}r$. V_i is the induced velocity, $\mathrm{d}L$ is the differential lift, and $\mathrm{d}D$ is the differential drag. The contribution of the blade element to F and Q is

$$\mathrm{d}F = \mathrm{d}L\cos(\phi + \alpha_i) - \mathrm{d}D\sin(\phi + \alpha_i), \tag{3}$$
$$\mathrm{d}Q/r = \mathrm{d}L\sin(\phi + \alpha_i) + \mathrm{d}D\cos(\phi + \alpha_i). \tag{4}$$

$\mathrm{d}L$ and $\mathrm{d}D$ can be calculated by

$$\mathrm{d}L = \frac{1}{2}\rho W^2 c \mathrm{d}r C_L, \tag{5}$$

$$\mathrm{d}D = \frac{1}{2}\rho W^2 c \mathrm{d}r C_D, \tag{6}$$

where c is the chord, C_L is the lift coefficient, and C_D is the drag coefficient. Let B be the number of the blades, then

$$\begin{aligned} F &= B\int \mathrm{d}F \\ &= B\int \left\{\mathrm{d}L\cos\left(\phi+\alpha_i\right) - \mathrm{d}D\sin\left(\phi+\alpha_i\right)\right\}, \end{aligned} \tag{7}$$

$$\begin{aligned} Q &= B\int \mathrm{d}Q \\ &= B\int r\left\{\mathrm{d}L\sin\left(\phi+\alpha_i\right) + \mathrm{d}D\cos\left(\phi+\alpha_i\right)\right\}. \end{aligned} \tag{8}$$

Considering the theoretical equations (5)–(8), C_F and C_Q are defined from experimental results as follows:

$$C_F = \frac{F}{\rho n^2 D_p^4}, \tag{9}$$

$$C_Q = \frac{Q}{\rho n^2 D_p^5}. \tag{10}$$

From Fig. 3, the angle of resultant flow ϕ is determined by the ratio of V and $2\pi nr$.

$$\tan\phi = \frac{V}{2\pi nr} = \frac{J}{\pi\frac{2r}{D_p}}. \tag{11}$$

J is defined by

$$J = \frac{V}{nD_p}. \tag{12}$$

Thus, C_F and C_Q are functions of J. F and Q can be written as

$$F = C_F(J)\rho n^2 D_p^4, \tag{13}$$

$$Q = C_Q(J)\rho n^2 D_p^5. \tag{14}$$

The equation of motion of the electric motor is

$$T - Q = 2\pi J_\omega \frac{\mathrm{d}n}{\mathrm{d}t} + 2\pi B_\omega n + T_C. \tag{15}$$

C. Tilt-Wing

As shown in (13) and (14), C_F and C_Q are functions of $J = \frac{V}{nD_p}$ when $\alpha = 0$. However, when $\alpha \neq 0$, C_F and C_Q become functions of J and α. Regarding this problem, it is experimentally shown that C_F and C_Q respectively become the same value when $J\cos\alpha$ is the same. In other words, C_F and C_Q become functions of only $J\cos\alpha$. Let J_n be

$$J_n = J\cos\alpha = \frac{V_n}{nD_p}, \tag{16}$$

F and Q can be written as

$$F = C_F(J_n)\rho n^2 D_p^4, \tag{17}$$

$$Q = C_Q(J_n)\rho n^2 D_p^5. \tag{18}$$

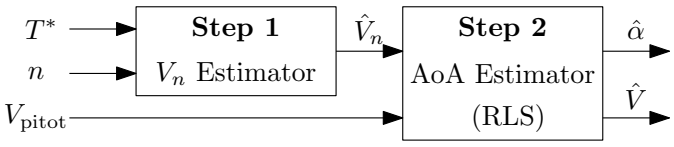

Fig. 4. Angle of attack estimator.

Forces acting on the wing and the propeller, F_x and F_z, are defined by L, D, and F. Let C_{F_x} and C_{F_z} be the coefficients, which are functions of α and J, F_x and F_z can be written as

$$F_x = C_{F_x}(\alpha, J)\,\rho V^2 S, \tag{19}$$

$$F_z = C_{F_z}(\alpha, J)\,\rho V^2 S. \tag{20}$$

As seen in (19) and (20), α is a critical parameter for aircraft motion.

D. Angle of Attack

The lift of an aircraft is calculated by

$$L = \frac{1}{2}\rho V^2 S C_L(\alpha), \tag{21}$$

$$C_L(\alpha) \simeq C_{L_\alpha}\alpha + C_{L_0}, \tag{22}$$

where C_L is the lift coefficient and S is the wing area. C_{L_α} and C_{L_0} are constants. When α exceeds the stall angle α_s, the airflow deviates and L drops rapidly. If L is assumed to be equal to the weight of the aircraft Mg, the stall speed V_s can be calculated by

$$V_s = \sqrt{\frac{2Mg}{C_{L_{\mathrm{Max}}}\rho S}}, \tag{23}$$

where $C_{L_{\mathrm{Max}}}$ is the maximum lift coefficient. Normally, aircraft are required to fly at $1.2V_s$ or faster while landing for safety reasons. In other words, if $C_{L_{\mathrm{Max}}} = C_L(\alpha_s)$, α has to be

$$\alpha \leq \frac{\alpha_s}{1.2^2} - \left(1 - \frac{1}{1.2^2}\right)\frac{C_{L_0}}{C_{L_\alpha}}. \tag{24}$$

When $C_{L_0} = 0$ and $\alpha_s = 13\,\mathrm{deg}$, (24) becomes $\alpha \leq 9\,\mathrm{deg}$. Therefore, AoA estimation accuracy needs to be at least $\pm 4\,\mathrm{deg}$ to avoid stall, and a more accurate estimation allows the use of a wider range of α.

III. Proposal of Observer-based Angle of Attack Estimaiton

In this section, the observer-based AoA estimation method is proposed. This method estimates both the airflow angle and magnitude (α and V). Since there are two estimation parameters, two sensors are needed: the pitot tube and motor torque. This method is based on propeller dynamics; therefore, a more direct estimation is achieved than the conventional estimation methods using IMU.

The proposed method consists of two steps. Step 1 is the observer-based airspeed estimation, and Step 2 is the AoA estimation using the recursive least-squares (RLS) method. The overall estimation flow is shown in Fig. 4.

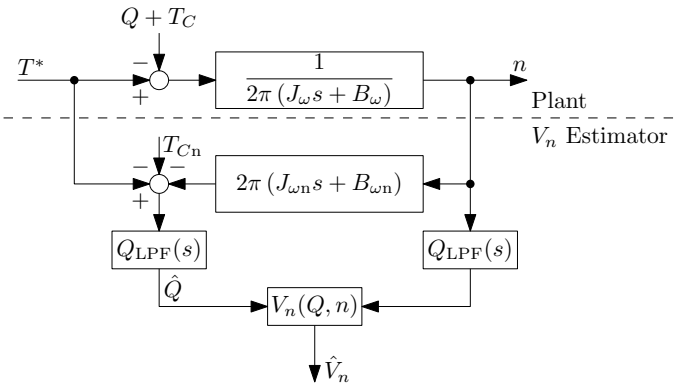

Fig. 5. Step 1: Normal airspeed estimator.

A. Step 1: Normal Airspeed Estimation

In Step 1, the observer-based V_n estimation method is proposed. The block diagram of V_n estimator is shown in Fig. 5. Since motor torque can be accurately estimated from motor current, V_n can be estimated from the motor current and propeller model. The idea of airspeed estimation using motor torque is proposed in [20] and adopted to the observer-based estimation scheme in [21], [22].

From (15), Q can be estimated using disturbance observer [23]–[25], as shown in Fig. 5. $C_Q(J_n)$ usually has an inverse function in the operating region. By using (16), (18), and the estimated value of Q, V_n can be estimated as follows:

$$\hat{V}_n = nD_p C_Q^{-1}\left(\frac{\hat{Q}}{\rho n^2 D_p^5}\right). \tag{25}$$

B. Step 2: Angle of Attack Estimation

Using Step 1 and V_x from the pitot tube, AoA is estimated in Step 2.

It seems possible to estimate AoA from (1) and (2); however, the pitot tube's sensor characteristic has to be considered, that is, $V_x \neq V_{\mathrm{pitot}}$ when $\sigma - \alpha \neq 0$. The relationship between $\sigma - \alpha$ and $\frac{V_{\mathrm{pitot}}}{V}$ of the test pitot tube is shown in Fig. 6. As seen in Fig. 6, $\frac{V_{\mathrm{pitot}}}{V}$ is not equal to $\cos(\sigma - \alpha)$.

There are several functions for fitting to this curve, such as the quadratic function. In this paper, both $\cos(\sigma - \alpha)$ and $\sin(\sigma - \alpha)$ were used for simplicity. Thus,

$$\frac{V_{\mathrm{pitot}}}{V} = a\cos(\sigma - \alpha) + b\sin(\sigma - \alpha), \tag{26}$$

where a and b are constant. a and b are determined by the least-squares method for the data above 20 deg. Since only trigonometric functions are used for AoA, this approximation simplifies the estimation equation (30).

From (1), (26), and Step 1,

$$\hat{V}_n = V\cos\alpha, \tag{27}$$

$$V_{\mathrm{pitot}} = V\left\{a\cos(\sigma - \alpha) + b\sin(\sigma - \alpha)\right\}. \tag{28}$$

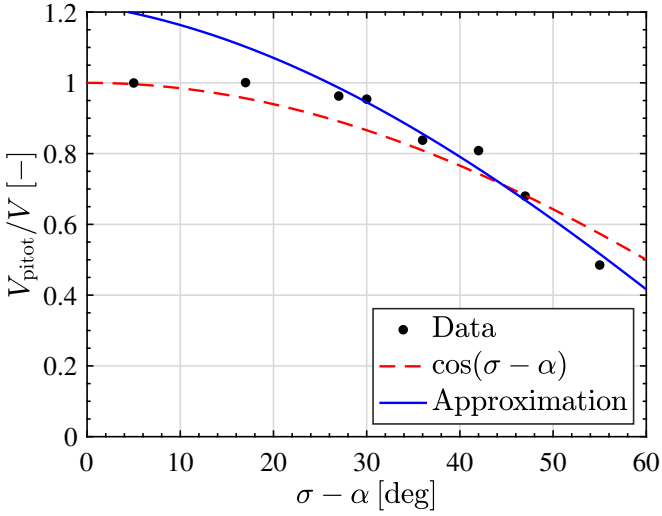

Fig. 6. Pitot tube's sensor characteristic.

Thus,

$$V_{\mathrm{pitot}} = \frac{\hat{V}_n}{\cos\alpha}\left\{a(\cos\sigma\cos\alpha + \sin\sigma\sin\alpha) + b(\sin\sigma\cos\alpha - \cos\sigma\sin\alpha)\right\}, \tag{29}$$

$$\therefore V_{\mathrm{pitot}} - \hat{V}_n(a\cos\sigma + b\sin\sigma) = \hat{V}_n(a\sin\sigma - b\cos\sigma)\tan\alpha. \tag{30}$$

As seen in (30), the estimation equation becomes a function of only $\tan\alpha$. Note that σ is a measurable parameter.

Step 2 uses RLS with a forgetting factor for noise reduction. In this estimation, the regression model is

$$y = \varphi\theta, \tag{31}$$

where output y, regressor φ, and estimation parameter θ are

$$y = Q_{\mathrm{LPF}}(s)V_{\mathrm{pitot}} - \hat{V}_n(a\cos\sigma + b\sin\sigma), \tag{32}$$

$$\varphi = \hat{V}_n(a\sin\sigma - b\cos\sigma), \tag{33}$$

$$\theta = \tan\alpha. \tag{34}$$

Updates of these parameters are calculated as follows:

$$\hat{\theta}[k] = \hat{\theta}[k-1] + \frac{P[k-1]\varphi[k]}{\lambda + P[k-1]\varphi^2[k]}\varepsilon[k], \tag{35}$$

$$\varepsilon[k] = y[k] - \varphi[k]\hat{\theta}[k-1], \tag{36}$$

$$P[k] = \frac{1}{\lambda}\left\{P[k-1] - \frac{P^2[k-1]\varphi^2[k]}{\lambda + P[k-1]\varphi^2[k]}\right\}. \tag{37}$$

Finally, estimated value of AoA $\hat{\alpha}[k]$ can be calculated by

$$\hat{\alpha}[k] = \arctan\hat{\theta}[k]. \tag{38}$$

The airflow magnitude V can be estimated by

$$\hat{V}[k] = \frac{\hat{V}_n[k]}{\cos\hat{\alpha}[k]}. \tag{39}$$

Fig. 7. Picture of experimental setup.

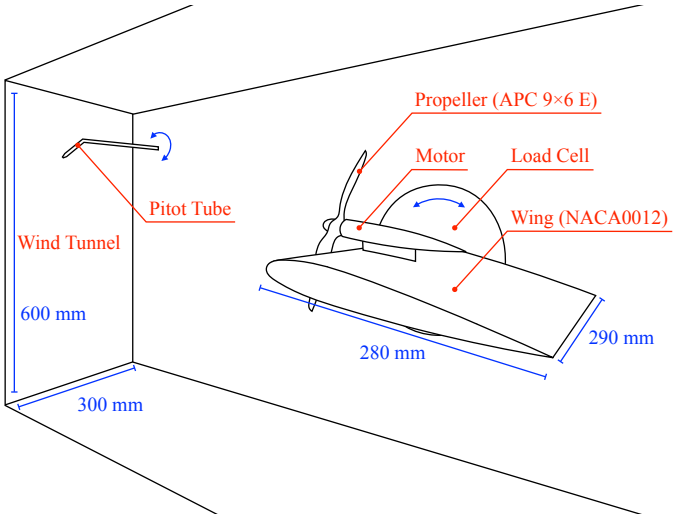

Fig. 8. Diagram of experimental setup.

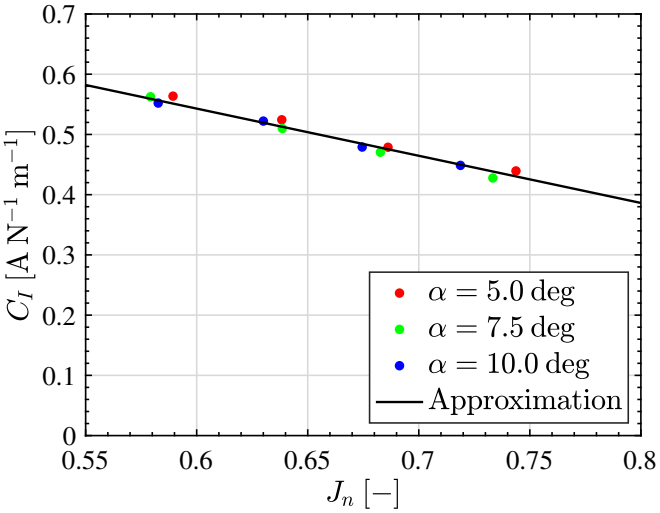

Fig. 9. Relationship between J_n and C_I.

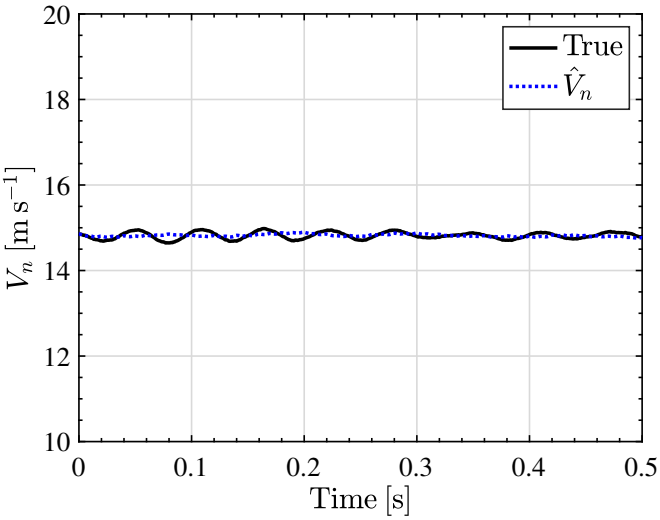

Fig. 10. Wind tunnel test result of Step 1.

IV. Experiment

In this section, the proposed method was verified by experiments in the wind tunnel.

A. Experimental Setup

Fig. 7 shows a picture and Fig. 8 shows a diagram of the experimental setup. The experimental unit consists of a pitot tube, a tiltable wing with an APC 9×6 E propeller, and a six-component load cell.

B. Experimental Result of Step 1

The relationship between current I and V_n was used in this experiment. Instead of using C_Q, a new coefficient C_I was defined by

$$C_I = \frac{I}{\rho n^2 D_p^5}. \tag{40}$$

The relationship between J_n and C_I tested at $V = 10\,\mathrm{m\,s^{-1}}$ is shown in Fig. 9. As seen in Fig. 9, C_I can be assumed to be function of only J_n for various α.

The wind tunnel test result of Step 1 is shown in Fig. 10. The cutoff frequency of $Q_{\mathrm{LPF}}(s)$ was 5 Hz, α was 10 deg, and $\sigma - \alpha$ was 0 deg. Also, I was filtered by a 50 Hz notch filter to reduce the power supply noise. From Fig. 10, it is shown that Step 1 achieved accurate V_n estimation.

C. Experimental Result of Step 2

Fig. 11 shows the wind tunnel test result of Step 2. α was 10 deg and $\sigma - \alpha$ was 47 deg. The sampling period was 1 ms. $\hat{\alpha}$ w/o RLS shows the result of solving (30) for each sample. The estimation with RLS started at 0.01 s. λ was 0.995, $\theta[0]$ was 0.178, and $P[0]$ was $10,000$ in this experiment. From Fig. 11, it is shown that Step 2 achieved accurate AoA estimation with little noise by Step 1 and RLS.

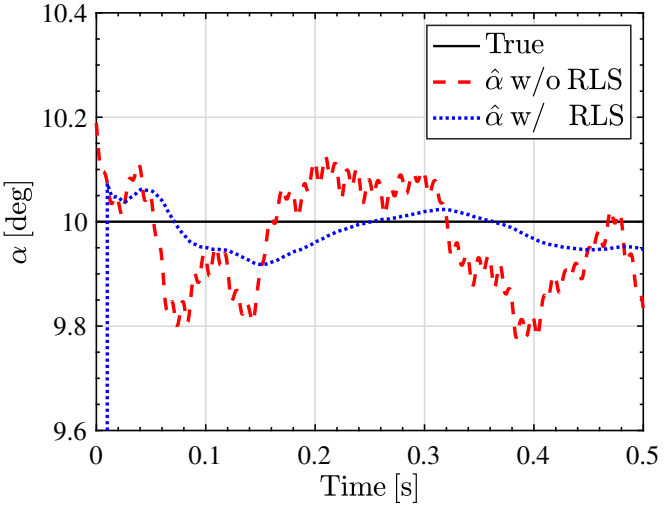

Fig. 11. Wind tunnel test result of Step 2.

V. Conclusion

eVTOL aircraft are attracting considerable attention as secure, efficient, and eco-friendly aviation. Especially, Tilt-Wing configuration is known as one of the efficient configurations. Tilt-Wing aircraft tend to be unstable during the transition from hover to cruise. In this study, a new observer-based AoA estimation method for Tilt-Wing aircraft was proposed to achieve stable transitions. The wind tunnel tests verified its effectiveness. Future work includes robust lift and thrust control using estimated AoA for the transition.

Acknowledgment

This work was partly supported by JSPS KAKENHI Grant Number JP18H03768.

References

[1] Y. Hori, "Future Vehicle Driven by Electricity and Control—Research on Four-Wheel-Motored "UOT Electric March II"," *IEEE Transactions on Industrial Electronics*, vol. 51, no. 5, pp. 954–962, oct 2004.

[2] N. K. Borer, M. D. Patterson, J. K. Viken, M. D. Moore, J. Bevirt, A. M. Stoll, and A. R. Gibson, "Design and Performance of the NASA SCEPTOR Distributed Electric Propulsion Flight Demonstrator," in *16th AIAA Aviation Technology, Integration, and Operations Conference*. Reston, Virginia: American Institute of Aeronautics and Astronautics, jun 2016, pp. 1–20.

[3] N. Adachi, H. Kobayashi, H. Hakojima, and A. Nishizawa, "An Experimental Study on Energy Regeneration Using Propellers," Tech. Rep., 2015, (in Japanese).

[4] K. Takahashi, H. Fujimoto, Y. Hori, H. Kobayashi, and A. Nishizawa, "Airspeed control of electric airplane based on 2-quadrant thrust control and verification with towing test using electric vehicle," in *IECON 2014 - 40th Annual Conference of the IEEE Industrial Electronics Society*. IEEE, oct 2014, pp. 2682–2688.

[5] N. Konishi, H. Fujimoto, Y. Watanabe, K. Suzuki, H. Kobayashi, and A. Nishizawa, "Lift control of electric airplanes by using propeller slipstream for safe landing," in *2015 IEEE International Conference on Mechatronics (ICM)*. IEEE, mar 2015, pp. 335–340.

[6] N. Konishi, H. Fujimoto, H. Kobayashi, and A. Nishizawa, "Range extension control system for electric airplane with multiple motors by optimization of thrust distribution considering propellers efficiency," in *IECON 2014 - 40th Annual Conference of the IEEE Industrial Electronics Society*. IEEE, oct 2014, pp. 2847–2852.

[7] H. Fujimoto and H. Sumiya, "Advanced safety range extension control system for electric vehicle with front- and rear-active steering and left- and right-force distribution," in *2012 IEEE/ASME International Conference on Advanced Intelligent Mechatronics (AIM)*. IEEE, jul 2012, pp. 532–537.

[8] W. Johnson, C. Silva, and E. Solis, "Concept Vehicles for VTOL Air Taxi Operations," in *AHS International Technical Meeting on Aeromechanics Design for Transformative Vertical Flight*, 2018.

[9] K. Muraoka, N. Okada, and D. Kubo, "Quad Tilt Wing VTOL UAV: Aerodynamic Characteristics and Prototype Flight," in *AIAA Infotech@Aerospace Conference*. Reston, Virigina: American Institute of Aeronautics and Astronautics, apr 2009.

[10] P. M. Rothhaar, P. C. Murphy, B. J. Bacon, I. M. Gregory, J. A. Grauer, R. C. Busan, and M. A. Croom, "NASA Langley Distributed Propulsion VTOL TiltWing Aircraft Testing, Modeling, Simulation, Control, and Flight Test Development," in *14th AIAA Aviation Technology, Integration, and Operations Conference*. Reston, Virginia: American Institute of Aeronautics and Astronautics, jun 2014.

[11] W. J. Fredericks, R. G. McSwain, B. F. Beaton, D. W. Klassman, and C. R. Theodore, "Greased Lightning (GL-10) Flight Testing Campaign," NASA, Tech. Rep., 2017.

[12] M. Sato and K. Muraoka, "Flight Controller Design and Demonstration of Quad-Tilt-Wing Unmanned Aerial Vehicle," *Journal of Guidance, Control, and Dynamics*, vol. 38, no. 6, pp. 1071–1082, jun 2015.

[13] P. Hartmann, C. Meyer, and D. Moormann, "Unified Velocity Control and Flight State Transition of Unmanned Tilt-Wing Aircraft," *Journal of Guidance, Control, and Dynamics*, vol. 40, no. 6, pp. 1348–1359, jun 2017.

[14] L. SANKARALINGAM and C. RAMPRASADH, "A comprehensive survey on the methods of angle of attack measurement and estimation in UAVs," *Chinese Journal of Aeronautics*, vol. 33, no. 3, pp. 749–770, mar 2020.

[15] P. Tian and H. Chao, "Model Aided Estimation of Angle of Attack, Sideslip Angle, and 3D Wind without Flow Angle Measurements," in *2018 AIAA Guidance, Navigation, and Control Conference*. Reston, Virginia: American Institute of Aeronautics and Astronautics, jan 2018.

[16] M. Oosterom and R. Babuska, "Virtual Sensor for the Angle-of-Attack Signal in Small Commercial Aircraft," in *2006 IEEE International Conference on Fuzzy Systems*. IEEE, 2006, pp. 1396–1403.

[17] P. Lichota and M. Lasek, "Maximum Likelihood Estimation: A method for flight dynamics - Angle of attack estimation," in *Proceedings of the 14th International Carpathian Control Conference (ICCC)*. IEEE, may 2013, pp. 218–221.

[18] T. A. Johansen, A. Cristofaro, K. Sorensen, J. M. Hansen, and T. I. Fossen, "On estimation of wind velocity, angle-of-attack and sideslip angle of small UAVs using standard sensors," in *2015 International Conference on Unmanned Aircraft Systems (ICUAS)*. IEEE, jun 2015, pp. 510–519.

[19] A. Wenz, T. A. Johansen, and A. Cristofaro, "Combining model-free and model-based angle of attack estimation for small fixed-wing UAVs using a standard sensor suite," in *2016 International Conference on Unmanned Aircraft Systems (ICUAS)*. IEEE, jun 2016, pp. 624–632.

[20] H. Kobayahi, A. Nishizawa, and T. Iijima, "Airspeed estimation by electric propulsion system parameters," in *55th Aircraft Symposium*. JSASS, 2017, (in Japanese).

[21] K. Yokota, H. Fujimoto, and Y. Hori, "Basic Study on Regenerative Air Brake Using Observer-based Thrust Control for Electric Airplane," in *2020 IEEE 16th International Workshop on Advanced Motion Control (AMC)*. IEEE, sep 2020, pp. 34–39.

[22] ——, "Descent Angle Control by Regenerative Air Brake Using Observer-based Thrust Control for Electric Aircraft," in *AIAA Propulsion and Energy 2020 Forum*. Reston, Virginia: American Institute of Aeronautics and Astronautics, aug 2020, pp. 1–13.

[23] K. Ohnishi, M. Shibata, and T. Murakami, "Motion control for advanced mechatronics," *IEEE/ASME Transactions on Mechatronics*, vol. 1, no. 1, pp. 56–67, mar 1996.

[24] S. Nagai, R. Oboe, T. Shimono, and A. Kawamura, "Fast Force Control without Force Sensor Using Combination of aaKF and RFOB for In-circuit Test with Probing System," *IEEJ Journal of Industry Applications*, vol. 8, no. 2, pp. 152–159, mar 2019.

[25] S. Yamada and H. Fujimoto, "Minimum-Variance Load-Side External Torque Estimation Robust Against Modeling and Measurement Errors," *IEEJ Journal of Industry Applications*, vol. 9, no. 2, pp. 117–124, mar 2020.